

## Deriving the coronal hole electron temperature: electron density dependent ionization / recombination considerations

John Gerard Doyle<sup>1</sup>, Steven Chapman<sup>2</sup>, Paul Bryans<sup>3,4</sup>, David Pérez-Suárez<sup>1</sup>, Avninda Singh<sup>1,5</sup>, Hugh Summers<sup>6</sup> and Daniel Wolf Savin<sup>7</sup>

<sup>1</sup> Armagh Observatory, College Hill, Armagh BT61 9DG, N. Ireland; *jgd@arm.ac.uk*

<sup>2</sup> Centre for Astrophysics, University of Central Lancashire, Preston, UK

<sup>3</sup> Space Science Division, Naval Research Laboratory, Washington, DC 20375, USA

<sup>4</sup> George Mason University, 4400 University Drive, Fairfax, VA 22020, USA

<sup>5</sup> Department of Physics & Electronics, Deen Dayal Upadhyaya College, University of Delhi, India

<sup>6</sup> Department of Physics, University of Strathclyde, 107 Rottenrow, Glasgow, G4 0NG, Scotland

<sup>7</sup> Columbia Astrophysics Laboratory, 550 W 120th St, New York, NY 10027, USA

Received 2009 August 7; accepted 2009 September 16

**Abstract** Comparison of appropriate theoretically derived line ratios with observational data can yield estimates of a plasma's physical parameters, such as electron density or temperature. The usual practice in the calculation of the line ratio is the assumption of excitation by electrons/protons followed by radiative decay. Furthermore, it is normal to use the so-called coronal approximation, i.e. one only considers ionization and recombination to and from the ground-state. A more accurate treatment is to include ionization/recombination to and from metastable levels. Here, we apply this to two lines from adjacent ionization stages, Mg IX 368 Å and Mg X 625 Å, which has been shown to be a very useful temperature diagnostic. At densities typical of coronal hole conditions, the difference between the electron temperature derived assuming the zero density limit compared with the electron density dependent ionization/recombination is small. This, however, is not the case for flares where the electron density is orders of magnitude larger. The derived temperature for the coronal hole at solar maximum is around 1.04 MK compared to just below 0.82 MK at solar minimum.

**Key words:** atomic processes — line: formation — Sun: activity

### 1 INTRODUCTION

Over the past few decades, many electron temperature and density diagnostics have been developed for application to observations of lines in the ultraviolet and extreme-ultraviolet regions of the spectrum, thereby providing insight to the physical parameters of the solar transition region and corona. The line ratio method usually involves a pair of lines from the same ion, although lines from adjacent ionization stages may be used. Thus, provided we have an accurate atomic model, the derived temperature provides essential data for an understanding of the basic processes occurring on the Sun.

Coronal holes, seen as regions with reduced emission due to a lower electron temperature than the surrounding quiet Sun, are an important source of open magnetic flux and high-speed solar

wind plasma. Furthermore, observing the evolution of coronal holes over the course of a solar cycle can lead to a better understanding of the solar dynamo and advance our knowledge in forecasting space weather. However, all this requires an effective method to detect and track coronal hole boundaries. Harvey & Recely (2002) used a hand-drawn method involving the He I 10830 Å line plus photospheric magnetic field data. This was further developed by Henney & Harvey (2005) and Malanushenko & Jones (2005) showing good agreement between the hand-drawn method and *SOHO/EIT* 195 Å images. With the amount and quality of EUV data currently available from *SOHO*, a few attempts have been made to develop a more automated method of coronal hole identification.

Scholl & Habbal (2008) used *SOHO/EIT* Fe IX/X 171 Å, Fe XII 195 Å and He II 304 Å, plus *SOHO/MDI* magnetograms. Chapman (2007) used EUV spectral line data obtained with *SOHO/CDS*. He showed that the ratios of Mg IX 368 Å and Mg X 625 Å resonance lines are an excellent temperature diagnostic for coronal holes, thus enabling a method not only to locate the coronal hole boundary but also an evaluation of the electron temperature with time. This work, however, employed the so-called coronal approximation, or zero-density approximation. This treats the populations of excited states of ions via an excitation balance of collisional excitation by electrons, and radiative decay. The ionization state is established as a balance of electron impact ionization from the ground state and radiative plus dielectronic recombination. In the simplest version of such modelling, secondary collisions with excited states are neglected.

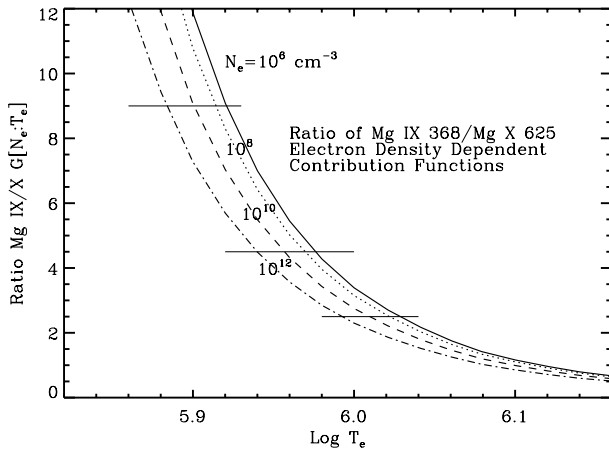


**Fig. 1** Ratio of the electron density dependent contribution functions for Mg IX 368 Å and Mg X 625 Å for four values of electron density ranging from very low densities to flare-type densities. The short horizontal lines at ratios of 1.0, 2.5 and 4.0 are the observed solar minimum, mean and maximum values, respectively (see Fig. 2).

Following from work by Burgess & Summers (1969) and Vernazza & Raymond (1979), it was shown by Doyle et al. (2005, 2006) that the contribution functions of resonance lines from low Z Be-like and Li-like ions can be altered substantially due to electron density dependent ionization considerations. Although we know that coronal holes are regions of reduced electron density compared to the quiet Sun, we do not know the extent of this additional atomic process with regard to Mg IX and Mg X.

Here, we investigate this dependence for Mg and apply it to the synoptic data obtained with *SOHO/CDS* (Harrison et al. 1995) as discussed by Chapman (2007) in order to access the extent of the electron density sensitivity in the Mg IX 368 Å and Mg X 625 Å lines.

## 2 CONTRIBUTION FUNCTION

An important component in calculating the line contribution function is the ionization balance. As would be expected from analyses of the solar corona, the so-called coronal approximation is most often implemented when calculating the ionization balance of the emitting plasma. In this approximation the plasma is considered optically-thin, low-density, dust-free, and in steady-state or quasi-steady-state. Under these conditions, the effects of any radiation field can be ignored, three-body collisions are unimportant, and the ionization balance of the gas is time-independent. The population of ionization stages is calculated as a balance of ionization due to electron impact ionization (EII) and recombination due to radiative recombination (RR) and dielectronic recombination (DR). The most recent compilation of the ionization balance under these conditions was by Bryans et al. (2009).

However, under certain conditions, the low-density approximation may not be appropriate as activity in the solar atmosphere can result in an increase in density where the coronal approximation breaks down. In the coronal approximation there is no treatment of metastable states with populations comparable to the ground state. In addition, the coronal approximation takes no account of secondary electron collisions. The generalized collisional-radiative picture (Summers & Hooper 1983) allows such an analysis. In detail, the collisional ionization and redistribution processes from excited states are included. The populated metastable states are determined via an elaborate ionization balance along with the ground states. These were computed within the Atomic Data and Analysis Structure (ADAS; Summers 2009<sup>1</sup>) framework, which is a collection of fundamental and derived atomic data, and codes that manipulate them.

Considering metastable level populations (including the ground level) to be dynamic and excited levels (i.e. all other levels) to be quasi-static, one can form population equations for each  $N_{\rho}^{(z)}$  and  $N_i^{(z)}$  in terms of these matrix elements as

$$\frac{dN_{\rho}^{(z)}}{dt} = C_{\rho\sigma} N_{\sigma}^{(z)} + C_{\rho j} N_j^{(z)} + C_{\rho\sigma+} N_{\sigma+}^{(z+1)} + C_{\rho\sigma-} N_{\sigma-}^{(z-1)}, \quad (1)$$

$$0 = C_{i\sigma} N_{\sigma}^{(z)} + C_{ij} N_j^{(z)} + C_{i\sigma+} N_{\sigma+}^{(z+1)} + C_{i\sigma-} N_{\sigma-}^{(z-1)}, \quad (2)$$

where we denote metastable states (including the ground state) by Greek indices and excited states by Roman indices. In the above, we use the summation convention over repeated indices. Such a matrix contains elements  $C_{\rho\sigma}$ ,  $C_{\rho j}$ ,  $C_{i\sigma}$ , and  $C_{ij}$  denoting the excitation (and de-excitation) rates between the respective levels;  $C_{\rho\sigma+}$  and  $C_{i\sigma+}$ , denoting the sum of the recombination rates from each metastable one; and  $C_{\rho\sigma-}$  and  $C_{i\sigma-}$ , denoting ionization rates; while the diagonal elements  $C_{\rho\rho}$  and  $C_{ii}$ , indicate total collisional and radiative loss rates from the levels  $\rho$  and  $i$ .

Recent work by Doyle et al. (2005, 2006) looked at this problem regarding formation of the resonance lines from low Z Li-like and Be-like ions. In the present work, we use ADAS to calculate the contribution functions of Mg IX 368 Å and Mg x 625 Å for different values of the electron density. The results of the ratio of these contribution functions are shown in Figure 1. We use the ionization and recombination data from ADAS in these calculations. The variation of the contribution functions is primarily due to the suppression of dielectronic recombination with increasing density as collisional depopulation of high  $n$ -shells, formed after stabilization, takes effect. This results in the ionization balance being shifted to lower temperatures and is reflected in the contribution function. In the next section, we apply the above results to recent coronal hole data.

## 3 OBSERVATIONAL DATA

The observational data used by Chapman and reproduced here (see Fig. 2) were the CDS synoptic study (SYNOP) which created two dimensional images and were run daily from around mid-night.

---

<sup>1</sup> <http://www.adas.ac.uk>

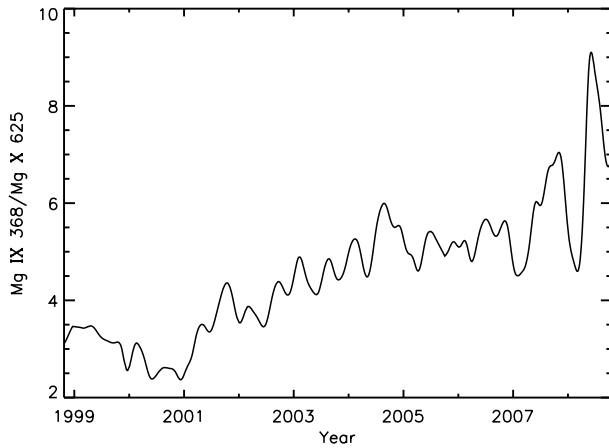


**Fig. 2** Observed ratio of Mg IX 368 Å to Mg X 625 Å from 1998 onwards as derived by Chapman (2007) smoothed over 28 d. The typical error on this smoothed data is less than 2%.

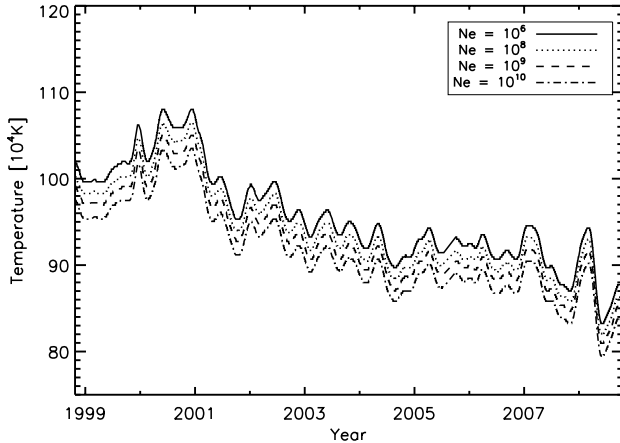


**Fig. 3** Derived electron temperature over a 9 year period from 1998 onwards for different electron densities. Note the lower temperature at solar minimum ( $\approx 2007/8$ ), while at solar maximum ( $\approx 2001/2$ ) there are intervals where the electron temperature is above 1 MK.

The study generated a series of nine rasters each of which covers a  $4 \times 4$  arcmin area. Together, the nine rasters spanned the central meridian of the Sun. The study used a selection of the strongest lines available in the CDS/NIS wavelength range, covering a wide range of temperatures from the chromosphere to the corona: He I 584 Å, O v 629 Å, Mg VII 367 Å, Mg IX 368 Å, Mg X 625 Å and Fe XVI 361 Å. As a result, a near-continuous dataset exists since 1996 which is well-suited to studying long-term variations in the solar structure. However, here we only use data taken after the *SOHO* recovery, i.e. from 1998, due to cross-calibration problems which are discussed in more

detail by Chapman (2007). Various methods used to extract the line fluxes, including background subtraction, use of small windows, line fitting, and calibration, are all discussed by Chapman (2007).

#### 4 RESULTS

At densities typical of coronal hole conditions (i.e.  $10^8 \text{ cm}^{-3}$  to  $10^9 \text{ cm}^{-3}$ , see Raymond & Doyle 1981), the difference of including ionization/recombination to/from metastable levels is small compared to the normal coronal approximation. This, however, is not the case for flares where the electron density can be orders of magnitude larger. In Figure 3, we show the derived electron temperature over a 9 year period from 1998 onwards for different electron densities. Note the lower temperature at solar minimum ( $\approx 2008$ ), while at solar maximum ( $\approx 2001$ ) there are intervals where the electron temperature is above 1 MK. Due to the high quality of the observational data, these observed changes, including not only the difference at solar minimum/maximum, but also the short-term changes throughout the cycle, are real. The paper by Chapman discusses in more detail the changes in the coronal hole coverage throughout the solar cycle, and its implications.

**Acknowledgements** Research at the Armagh Observatory is grant-aided by the Northern Ireland Department of Culture, Arts and Leisure. We thank the UK Science and Technology Facilities Council for support via ST/F001843/1. *SOHO* is a mission of international cooperation between ESA and NASA. PB was supported in part by the NASA Solar and Heliospheric Physics Supporting Research and Technology program. We thank A. Whiteford for his guidance on using ADAS. JGD thanks the International Space Science Institute, Bern for the support of the team “Small-scale transient phenomena and their contribution to coronal heating.”

#### References

- Bryans, P., Landi, E., & Savin, D. W. 2009, ApJ, 691, 1540  
 Burgess, A., & Summers, H. P. 1969, ApJ, 157, 1007  
 Chapman, S. A. 2007, PhD thesis, University of Central Lancashire, Preston, UK  
 Doyle, J. G., Summers, H. P., & Bryans, P. 2005, A&A, 430, L29  
 Doyle, J. G., Ishak, B., Madjarska, M. S., O’Shea, E., & Dzifcákova, E. 2006, A&A 452, L35  
 Harrison, R. A., et al. 2005, Solar Phys., 162, 233  
 Harvey, K. L., & Recely, F. 2002, Solar Phys., 211, 31  
 Henney, C. J., & Harvey, J. W. 2005, in ASP Conf. Ser. 346, Large-scale Structures and their Role in Solar Activity, eds. K. Sankarasubramanian, M. Penn, & A. Pevtsov (San Francisco, CA: ASP), 261  
 Malanushenko, O. V., & Jones, H. P. 2005, Solar Phys., 226, 3  
 Raymond, J. C., & Doyle, J. G. 1981, ApJ, 247, 686  
 Scholl, I. F., & Habbal, S. R. 2008, Solar Phys., 248, 425  
 Summers, H. P., & Hooper, M. B. 1983, Plasma Physics, 25, 1311  
 Summers, H. P. 2009, The ADAS User Manual, version 2.6 (<http://www.adas.ac.uk/manual.php>)  
 Vernazza, J. E., & Raymond, J. C. 1979, ApJ, 228, L89